Local chemical order in a $(Ni_3Fe)_{0.93}Cr_{0.07}$ single crystal

A. Marty
Département de Recherches sur la Fusion Contrôlée, Centre d'Études Nucléaires de Grenoble, SPMM MP, 85X, 38041 Grenoble Cdeex, France and Centre d'Études de Chimie Métallurgique, Centre National de la Recherche Scientifique, 15 Rue G. Urbain, F-94407 Vitry-sur-Seine Cedex, France

P. Cenedese
Centre d'Études de Chimie Métallurgique, Centre National de la Recherche Scientifique, 15 Rue G. Urbain, F-94407 Vitry-sur-Seine Cedex, France

M. Bessiere and S. Lefebvre
Laboratoire pour l'Utilisation du Rayonnement Électromagnétique, Batiment 209D, Université Paris-Sud, 91405 Orsay Cedex, France

Y. Calvayrac
Centre d'Études de Chimie Métallurgique, Centre National de la Recherche Scientifique, 15 Rue G.Urbain, F-94407 Vitry-sur-Seine Cedex, France

(Received 28 December 1993; revised manuscript received 1 March 1994)

In a ternary alloy, there are three independent pair-correlation functions for each orbit. Diffraction experiments cannot extract this information unless variations in the scattering factors of each atomic species are exploited. Such an experiment, using x-ray anomalous scattering with a synchrotron radiation, is described in this paper on a $(Ni_3Fe)_{0.93}Cr_{0.07}$ single crystal. Due to the small amount of Cr, only two pair-correlation functions have been obtained directly from the diffraction data. The missing information has been supplied using an original method based on the inverse cluster variation method. As a by-product, the method gives plausible effective pair potentials which have been used in Monte Carlo simulations. Atom distributions of the alloy and intensity maps of the diffuse scattering are calculated as a function of the temperature, through the order-disorder transition. The method used opens a way towards a better knowledge of ternary alloys, for which very few direct determinations of the degree and nature of the ordering are possible.

I. INTRODUCTION

The ordering of atoms in alloys has a great influence on their properties. Both the ordering and the way the properties are subsequently affected are controlled by interaction energies. These have to be known before any modeling, and hence any optimization of the composition in order to obtain the properties desired, can be achieved.

In an Ising like model, effective pair potentials are defined for each kind of heterogeneous atomic pair and each coordination shell:

$$J_n^{ij} = \frac{V_n^{ii} + V_n^{jj} - 2V_n^{ij}}{4},$$

where V_n^{ij} is the pair interaction energy between nth neighbors i and j atoms.

These effective pair potentials can be determined from x-ray or neutron diffuse scattering measurements on short-range ordered single crystals.

In a solid solution where the different kinds of atoms are randomly distributed on the lattice, x-ray-diffraction produces a monotonic diffuse intensity, the so-called "Laue monotonic diffuse scattering." The presence of local order causes the Laue diffuse intensity to be modulated and a study of this modulation leads to the determination of the Warren-Cowley short-range order (SRO) parameters:

$$\alpha^{ij}(\mathbf{r}) = 1 - \frac{P^{ij}(\mathbf{r})}{C_i C_j},$$

where C_i, C_j are the atomic fractions of i and j atoms in the solid solution and $P^{ij}(\mathbf{r})$ is the probability of finding the i and j atoms in a pair separated by a lattice vector $\mathbf{r}$. The short-range order parameters are then direction dependent except for temperatures very close to the critical temperature, where the correlation length behaves isotropically. From the SRO parameters, effective interaction potentials can be calculated using thermodynamic methods such as the inverse Monte Carlo method[1] or the inverse cluster variation method (ICVM).[2]

The distribution of atoms in solid solutions is in general not random and a number of structural data have been accumulated on a variety of binary alloys. On the other hand, there have been very few investigations on ternary alloys, due to severe difficulties involved: three atomic pair correlation functions per shell are required to describe the SRO state in ternary alloys, in contrast to just one in binaries, so special experimental techniques have

to be used. To the knowledge of the authors, such measurements have been performed only two times: on the $Fe_{0.56}Ni_{0.23}Cr_{0.21}$ alloy, by neutron diffraction on three single crystals with different isotopic compositions,[3] and on a $Cu_{0.47}Ni_{0.29}Zn_{0.24}$ single crystal, using x-ray anomalous scattering phenomenon with a synchrotron radiation source.[4]

We present here a study of the SRO state in a $(Ni_3Fe)_{0.93}Cr_{0.07}$ single crystal, using the anomalous scattering method. This alloy was selected for both scientific and technical reasons: (i) Ni_3Fe is the basis of a number of important magnetic alloys and chromium is widely used as a third component. However, the nature of short-range order in these alloys has still not been determined, the structural data having mainly been obtained by indirect methods (Mössbauer spectrometry, resistivity). (ii) Diffuse scattering measurements on Fe-Cr (Refs. 5 and 6), Ni-Cr (Refs. 7–9), and Ni-Fe (Ref. 10) binary alloys and on a Fe-base Fe-Ni-Cr alloy (Ref. 3) have been reported in the literature and these data can be used for a comparison. (iii) The atomic size differences between Ni, Cr, and Fe are small, and size effect scattering is expected to be negligible. Indeed the neutron diffraction study of Lefebvre *et al.*[10] showed that, in a $Ni_{0.765}Fe_{0.235}$ single crystal quenched from 535 °C, the atomic displacement parameters are very small. However, in a very nice experiment using an anomalous-x-ray-diffraction procedure on a $Ni_{0.775}Fe_{0.225}$ single crystal, Ice *et al.*[11] recently showed obvious displacement parameters about 10 times stronger, beside similar SRO coefficients. Anyway, in the work reported here, the measurements are made in the first Brillouin zone where the size effect intensity remains small and can be neglected to a first approximation. (iv) The use of anomalous scattering can be optimized because wavelengths near the absorption thresholds of the three elements of the alloy are available with the synchrotron radiation source of LURE-DCI (the wavelength range available for diffuse scattering intensity measurements extends from 1 to 2.5 Å). Several studies have shown that Cr additions in Ni_3Fe rapidly destroy the long-range order (LRO), which changes to a SRO state. Ferjani, Bley, and Calvayrac,[12] using x-ray diffraction, determined the order-disorder transition temperature T_c of $(Ni_3Fe)_{1-x}Cr_x$ alloys for values of x up to 1.5% and Marwick, Piller, and Cranshow,[13] using Mössbauer spectrometry, have extended these studies to concentrations x up to 17%. Marwick, Piller, and Cranshow,[13] using electron irradiation to increase the ordering rate, have detected LRO up to 6.1 at. % Cr. This result is consistent with the results of Gomankov and Nogin[14] who showed by neutron diffraction that LRO extends only to 6 at. % Cr.

In the Ni-Fe-Cr system the fcc solid solution range is large, so it was expected that Cr-rich alloys might be studied, in order to obtain sufficient partial diffuse intensity arising from the Fe-Cr correlations. However, preliminary diffuse scattering intensity measurements on $(Ni_3Fe)_{1-x}Cr_x$ single crystals with $x = 0.04$, 0.07, and 0.10 showed that the diffuse intensity rapidly decreases when Cr is added, and we had to limit our study to the single crystal with 7 at. % Cr. As we shall see below, this Cr content does not allow the direct determination of all three independent correlation functions, only the two corresponding to the majority pairs Ni-Fe and Ni-Cr may reliably be obtained. Hence we have tried to extract the lacking information from thermodynamic consistency considerations using other independently obtained data. A thermodynamic study of order in dilute $L1_2$-ordered ternary alloys[15] has provided relationships between both the variation of the transition temperature T_c and that of the LRO parameter of the ternary addition η_C and the same linear combination of the effective potentials. We shall see that using these relationships, together with available value of the LRO parameter for Cr measured in a long-range ordered $(Ni_3Fe)_{0.96}Cr_{0.04}$ sample,[16] we have succeeded in determining a "plausible" set of SRO parameters for the Fe-Cr pairs, as well as effective pair interaction potentials.

II. GENERAL EQUATIONS

For a given scattering vector $\mathbf{q}$, the SRO diffuse scattering intensity per site for a ternary alloy can be written in electron units as follows:

$$\begin{aligned} I_{\mathrm{SRO}}(\mathbf{q}) = {} & C_A C_B \mid f_A - f_B \mid^2 \alpha^{AB}(\mathbf{q}) \\ & + C_A C_C \mid f_A - f_C \mid^2 \alpha^{AC}(\mathbf{q}) \\ & + C_B C_C \mid f_B - f_C \mid^2 \end{aligned}$$

where f_A is the atomic scattering factor of the element A. The functions $\alpha^{ij}(\mathbf{q})$, in Laue units, are partial diffuse intensities resulting from the three kinds of interatomic correlations, AB, AC, and BC. These partial intensities are the Fourier transforms of the Warren Cowley parameters for the three kinds of pairs:

$$\alpha^{AB}(\mathbf{q}) = \sum_{k,l,m} \alpha^{AB}(\mathbf{r}_n)\, e^{2i\pi \mathbf{q}\cdot\mathbf{r}_n},$$

$$\mathbf{r}_n = k\frac{\mathbf{a}_1}{2} + l\frac{\mathbf{a}_2}{2} + m\frac{\mathbf{a}_3}{2},$$

$$k + l + m = 2p,$$

where $\mathbf{a}_1, \mathbf{a}_2, \mathbf{a}_3$ are the unit cell vectors and k, l, and m are integers summing on even numbers. In order to determine the three correlation functions we have to obtain a system of at least three independent and well-conditioned equations. The scattering contrast was varied using the sharp variation of the atomic scattering factors for incident energies near the absorption edges of the elements. Figure 1 shows the behavior of the three Laue factors $C_iC_j \mid f_i - f_j \mid^2$ as a function of the x-ray wavelength, for the $(Ni_3Fe)_{0.93}Cr_{0.07}$ alloy for $\mathbf{q} = [100]$. The Laue factors rapidly vary close to the absorption edges, however, owing to the low product $C_{\mathrm{Fe}}C_{\mathrm{Cr}}$, the Laue factor for the Fe-Cr pairs always remains small compared to the others, so that the Fe-Cr correlations will be masked. Hence, we have first considered that only the Ni-Fe and Ni-Cr pair correlations contributed significantly to the diffuse scattering, and we have estimated the effect of

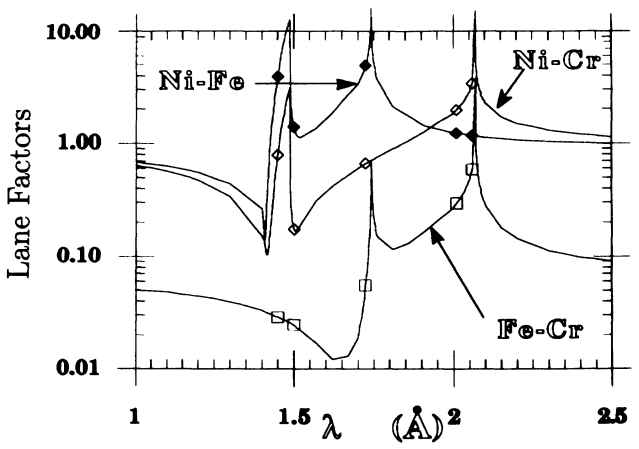

FIG. 1. Laue factors $C_iC_j \mid f_i - f_j \mid^2$ for the three partial intensities, as a function of the x-ray wavelength, for $(Ni_3Fe)_{0.93}Cr_{0.07}$ ($\mathbf{q} = [100]$).

this approximation on our results. Under this assumption, experiments near Fe and Cr edges are sufficient, leading to a well-defined linear system of equations from which SRO parameters for Ni-Fe and Ni-Cr pairs are accurately determined.

III. EXPERIMENTAL

A. Sample preparation

The single crystal was grown in an alumina crucible under a purified argon atmosphere using a Bridgman technique. The purity of the elements was 99.95%. The crystal was annealed for 48 h at 1623 K under a purified argon atmosphere for homogenization. It was then cut by spark erosion to obtain a disk of 20 mm diameter with a normal close to the ⟨112⟩ direction. The surface was mechanically polished then electropolished to remove any surface damage.

The disk was sealed in vacuum in a pyrex tube, annealed at 767 K for 18 h, then at 723 K for four days, and quenched in ice water. This annealing temperature was chosen as being slightly above the critical temperature (718 K) estimated from the results of Marwick, Piller, and Cranshow.[13] The sample was electropolished after this heat treatment, to remove a thin oxide film.

The sample was examined by scanning electron microscopy in a Zeiss DSM-950 equipped with an energy dispersive x-ray spectroscopy system (TRACOR Northern TN 5450) with a Si-Li detector. This analysis confirmed the nominal composition to within 0.2% and showed that the homogeneity of the Cr concentration was better than 0.2% over the area irradiated during the experiment.

B. Diffuse scattering intensity measurements

The intensity measurements were performed on the four circle goniometer set up on the OD23O beam line at LURE-DCI (Laboratoire pour l'Utilisation du Rayonnement Electromagnétique, Orsay-France). The beam line is equipped with a double crystal (Si⟨111⟩) fixed-exit monochromator. The second crystal is bent to horizontal beam focusing. The sample is maintained under an evacuated beryllium hemisphere, fixed on a goniometer head. The Si-Li solid-state detector has an energy resolution of 200 eV. The chosen wavelengths were adjusted by reference to extended x-ray-absorption fine structure (EXAFS) spectra from Cu, Ni, and Cr foils. The accuracy of the energy determination is 2 eV, so the wavelengths are measured within an accuracy of 2×10^{-4} Å. The instabilities of the incident monochromatic beam are automatically corrected by a monitor detector, which records the diffuse scattering from a Kapton foil.

This spectrometer has been described in detail elsewhere.[17] An important instrumental modification was necessary to carry out our experiment. The first diffuse scattering intensity measurements on the sample showed that appreciable amounts of harmonics $\frac{\lambda}{3}$ and $\frac{\lambda}{4}$ in the beam produce fluorescent radiations from the elements of the alloy. These radiations have wavelengths close enough to the fundamental wavelength for them to be counted. This causes a uniform increase in the background intensity, which cannot be measured and subtracted because it evolves during experiments: as a matter of fact, the amount of harmonics in the beam depend sensitively on the orientation of the second crystal of the monochromator, which deviates slightly as time goes on. The technical solution has consisted in mounting, after the monochromator, a flat double mirror oriented for cutting energies greater than 10 keV.[18] For the material used (borosilicate) the critical angle is 3 mrad at 10 keV.

The diffuse intensity was measured through a volume in the reciprocal space bounded by the (111),(100),(110),$\frac{1}{2}$(111) positions. This is the minimum volume nearest to the origin in which intensity has to be measured to determine the SRO parameters when no account is taken of any static displacement effect.[19] The diffuse intensity was measured over 160 points in this volume; the mesh interval used was $\Delta h = 0.1$ in reciprocal lattice units. Within this volume, the measurements are done for low values of the magnitude of the scattering vector, so the contribution to the diffuse scattering intensity of Compton scattering, thermal scattering and static displacement effects are minimized.

As stated above, we considered that the static displacement effects could be neglected, the atomic radii of the three elements being nearly the same. In order to ascertain whether this assumption was valid, we measured the diffuse intensity along a $[h, 0, 0]$ direction (Fig. 2). There are neither a shift nor asymmetry around the (300) position, which supports the absence of static displacement effects in this alloy.

The measurements were made at 100 K in order to minimize dynamic displacement effects due to thermal vibration of the atoms. The diffuse intensity was measured using a set of five wavelengths close to the K absorption edges of Fe and Cr: 1.7458, 1.7587 , 2.0720, 2.0734, and 2.0803 Å.

C. Data analysis

The measured intensity was converted into absolute electron units, from the integrated intensities of Bragg

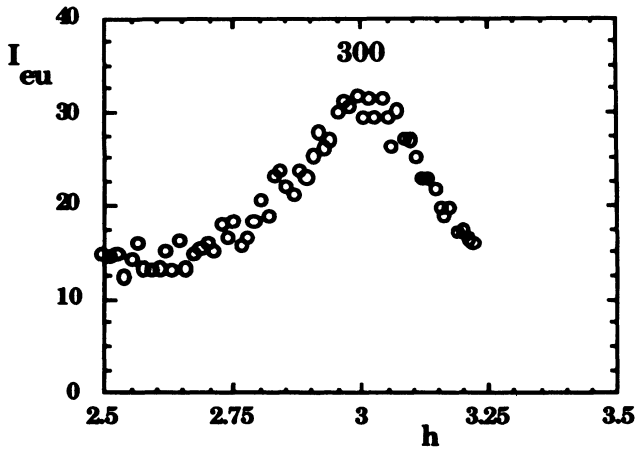

FIG. 2. Experimental intensity in electron units in a [h00] direction, around the (300) position.

peaks from a compacted Al powder reference sample. The scattering factors f_0 were taken from Doyle and Turner[20] and the anomalous scattering corrections $\Delta f'$ and $\Delta f''$ from Sasaki.[21] The Compton inelastic scattering, calculated from Cromer and Mann[22] and Cromer,[23] was then subtracted.

The thermal diffuse scattering (TDS) was minimized by making the measurements at low temperature and as near as possible to the reciprocal space origin. The TDS contribution is usually calculated from experimental lattice dynamics data following Walker and Chipman.[24] The validity of this calculation depends on the assumption that the average energy of the elastic waves is kT for each wave, so that the energy is equally distributed over all the normal modes. This assumption is valid when the measurements are made at a temperature T, which is high with respect to the Debye temperature Θ_D. For Ni_3Fe, $\Theta_D = 450\,K$,[25] while our measurements were carried out at $T = 100$ K. As the basic assumption of Walker and Chipman[24] is not met, we have estimated the TDS contribution from the calculation given in the Appendix. It shows that the scattering factors have to be weighted by a factor $\sqrt{\frac{m}{m_A}}$ in the expression of the first-order term of the thermal diffusion intensity, where the averaged mass m is given by $m = \sum c_A m_A$ if m_A is the atomic mass of species A. The knowledge of the elastic constant being part of the calculation, we used the data measured by Turchi, Calvayrac, Plique[25] on a Ni_3Fe crystal: $C_{11} = 25 \times 10^{10}\ Pa$, $C_{12} = 15 \times 10^{10}\ Pa$, and $C_{44} = 12 \times 10^{10}\ Pa$. Each value of the measured intensity was corrected for its first-order thermal diffuse scattering component.

In addition to these contributions, a residual background remains due to fluorescence from the sample and resonant Raman scattering: in the experimental conditions we used, when the energy of the incident radiation is just below the absorption edge of an element, the resonant Raman scattering has an appreciable cross section. In some experiments, due to the limited resolution of the detecting system (about 200 eV), a fraction of these unwanted contributions is counted and this generates a uniform residual background that depends both on the incident radiation wavelength and on the setting of the pulse-height analyzer of the detector. We have therefore considered it as an additional unknown for each wavelength.

The final corrections to the intensity deal with the Bragg peak intensity cutoff. In the volume we considered, all the measured intensities within a sphere of radius $|q_c|$ around the position of the (111) Bragg peak were removed. As the SRO parameters were determined through a least-squares fitting method and as we set $|q_c|$ small enough, it was unnecessary to extrapolate the data under the Bragg peaks.

IV. RESULTS

The value of α_0 was taken as unity for each pair, while the higher-order SRO parameters were obtained by least-squares analysis of a linear system, which is overdetermined insofar as the range of local order is short (see Sec. V). Weights were given to each equation inversely proportional to $\sqrt{I_{\text{measured}}}$.

The number of unknown parameters depend on the number $n_{\max}$ of orbits taken into account. We give in Fig. 3, the first ten parameters as a function of $n_{\max}$, for

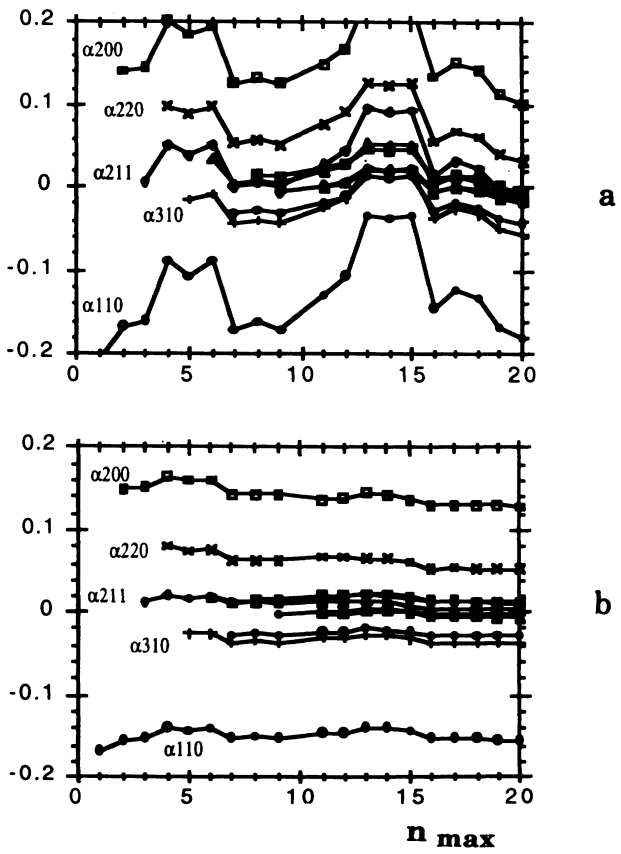

FIG. 3. The first ten α^{Ni-Fe} SRO parameters as a function of the number of orbits taken into account ($n_{\max}$), for two values of the cutting radius ($|\mathbf{q}_c|$) around the Bragg peaks: (a) $|\mathbf{q}_c| = 0.35$ and (b) $|\mathbf{q}_c| = 0.20$.

two values of the cutting radius $|q_c|$. Each α parameter oscillates on both sides of a mean value, with an amplitude depending on $|q_c|$. Therefore, we used a value $|q_c^*|$ equal to 0.2 that minimizes the oscillations. Given $|q_c^*|$, the agreement ratio between the measured intensities and the intensities reconstructed from the set of α's, was found insensitive to $n_{\max}$ beyond the sixth orbit. Hence we limited $n_{\max}$ to ten, and 25 unknown parameters were considered: 20 SRO parameters including Ni-Fe and Ni-Cr pairs and 5 residual backgrounds.

The set of α's obtained are given in Table I and are plotted in Fig. 4, and in Fig. 5 as a function of the orbit, with error bars estimated from the statistical errors in the intensities. An example of the measured SRO intensity is shown in Fig. 6(a), for a wavelength $\lambda = 1.7458$ Å(10 eV below the absorption edge of Fe), along with the reconstructed intensity in Fig. 6(b).

For the Ni-Fe pairs, the sign of the set of SRO parameters oscillates in the same way as in a $L1_2$ superstructure. The values of α, as well as the range of SRO, are quite similar to those determined by Lefebvre *et al.*[10] on a Ni_3Fe single crystal quenched from 808 K, which are also listed in Table I for comparison: thus the addition of 7 at. % Cr in Ni_3Fe does not affect the ordering behavior for the Ni-Fe pair.

For the Ni-Cr atomic pair, the evolution of the α's as a function of the shell number is clearly different and qualitatively reflects the behavior associated with a DO_{22} long range ordered state. This result can be compared with the result obtained by Schönfeld *et al.*[7] by neutron scattering on a $Ni_{0.80}Cr_{0.20}$ single crystal annealed at 741 K and water quenched (see Table I). For the first three α, the sequence of the sign is the same. However, in this binary alloy, as pointed out by the authors, the sign sequence for the whole set of α's corresponds to the A_2B_2 long-range ordered structure. The α values obtained by Sarfati,[9] on a Ni_3Cr crystal measured at 833 K, are in excellent agreement with those of Schönfeld *et al.*[7]

V. PLAUSIBLE α FROM THERMODYNAMIC SELF-CONSISTENCY

In the Introduction, we pointed out that the fundamental physical parameters, which need determining are the

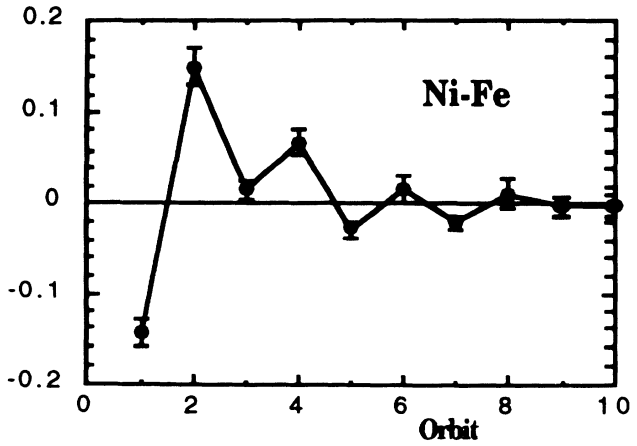

FIG. 4. Warren-Cowley SRO parameters for the Ni-Fe pair.

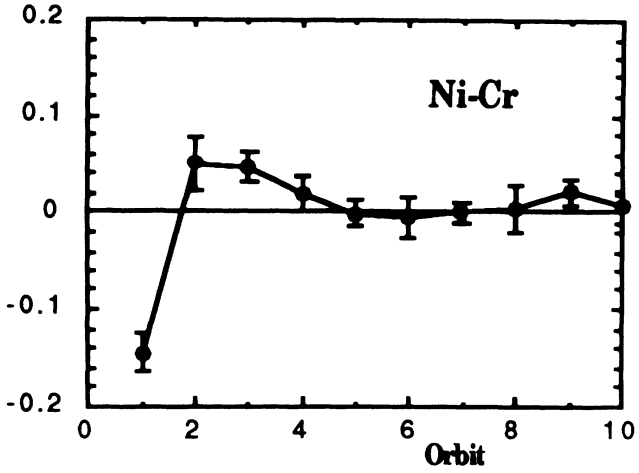

FIG. 5. Warren-Cowley SRO parameters for the Ni-Cr pair.

effective potentials. From the potentials we can attempt to calculate the ground-state energy, antiphase boundary (APB) or interphase boundary (IPB) excess free energy, or the local topology of the phase diagram. There are several ways to achieve this goal.

Because the diffuse scattering intensity forms a part of the Fourier spectrum of the correlation functions, there is a direct link between the J's and the diffuse intensity. In binary alloys the famous Clapp and Moss[26] formulas gives an explicit simple example of such methods, when the basic cluster of the CVM is taken to be a point. The accuracy of the method can be improved further, using larger clusters, as shown by Sanchez.[27] The main advantage of the method is that fewer parameters (the J's) are used to fit the intensities, and that once these parameters have been determined, the set of α parameters can be obtained directly from an exact Fourier transform.[28] However, owing to the splitting of binary correlation functions, the method starts to be very heavy in mul-

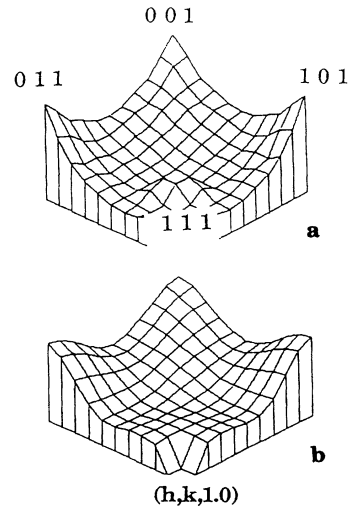

FIG. 6. Distribution of the SRO diffuse scattering intensity in reciprocal space for $\lambda = 1.7458$ Å(Fe edge): (a)measured and (b)reconstructed from the α's.

TABLE I. SRO parameters α_{lmn} for the Ni-Fe and Ni-Cr atomic pairs in the $(Ni_3Fe)_{0.93}Cr_{0.07}$ alloy along with the results obtained for binary alloys: $Ni_{0.765}Fe_{0.235}$ (Ref. 10) and $Ni_{0.80}Cr_{0.20}$ (Ref. 7).

	$(Ni_3Fe)_{0.93}Cr_{0.07}$		$Ni_{0.765}Fe_{0.235}$	$Ni_{0.80}\ Cr_{0.20}$
lmn	$\alpha_{Ni\text{-}Fe}$	$\alpha_{Ni\text{-}Cr}$	$\alpha_{Ni\text{-}Fe}$	$\alpha_{Ni\text{-}Cr}$
110	-0.143 ± 0.015	-0.141 ± 0.020	-0.111	-0.106
200	$+0.149 \pm 0.019$	$+0.050 \pm 0.026$	$+0.136$	$+0.089$
211	$+0.015 \pm 0.011$	$+0.046 \pm 0.015$	-0.006	$+0.042$
220	$+0.068 \pm 0.013$	$+0.020 \pm 0.018$	$+0.052$	-0.036
310	-0.029 ± 0.010	-0.002 ± 0.014	-0.022	-0.019
222	$+0.016 \pm 0.015$	-0.005 ± 0.021	$+0.031$	-0.034
321	-0.021 ± 0.008	$+0.000 \pm 0.011$	-0.014	$+0.007$
400	$+0.010 \pm 0.017$	-0.004 ± 0.023	$+0.022$	$+0.029$
411	-0.003 ± 0.010	$+0.022 \pm 0.013$	-0.013	$+0.003$
330	-0.002 ± 0.013	$+0.006 \pm 0.017$	-0.013	$+0.022$

ticomponent alloys where rather small clusters should be considered.[28]

In this section, we address ourselves to the same problem, but using a more unusual feature of the CVM, based on the internally self-consistent character of the Ising model. In other words, calculate the J's will allow us to define a plausible set of α's even when the information relative to one pair is experimentally masked, as it is the case here for the Fe-Cr pair.

To answer this question, we will begin by describing the least-squares procedure in some detail. As mentioned in the previous paragraph, we have to solve an over-estimated set of linear equations, given by

$$I_{\mathrm{eu}}(\mathbf{q},\lambda) - \sum_{i,j>i} L_i^j(\mathbf{q},\lambda) = B(\lambda) + \sum_{i,j>i} L_i^j(\mathbf{q},\lambda) \sum_{n}^{n_{\max}} F_n(\mathbf{q})\,\alpha_n^{ij}, \quad (1)$$

where $I_{\mathrm{eu}}(\mathbf{q},\lambda)$ is the SRO intensity in electron units for wavelength λ at position $\mathbf{q}$ $L_i^j(\mathbf{q},\lambda)$ is the Laue factor of the pair i-j, $B(\lambda)$ is the residual background considered as an unknown, and $F_n(\mathbf{q})$ is the nth lattice generating function. The Laue factor $L_{\mathrm{Fe}}^{\mathrm{Cr}}(\mathbf{q},\lambda)$ of the Fe-Cr pair being small with respect to the Laue factors of the two other pairs, we first look for the solution of Eq. (1), assuming that $\alpha_n^{\mathrm{Fe\text{-}Cr}} = 0$ for all $n \geq 1$. Let the row vectors $\boldsymbol{\alpha}_0^{ij} = \left(\alpha_1^{ij}, \alpha_2^{ij}, \ldots, \alpha_{\max}^{ij}\right)$ represent the corresponding solution. In a second stage, we try to quantify the variations of the previous solution vector $\delta\boldsymbol{\alpha}_0^{ij}$ on variations of the unknown parameters $\delta\boldsymbol{\alpha}^{\mathrm{Fe\text{-}Cr}}$. It follows from Eq. (1), that the perturbations of our initial guess $\boldsymbol{\alpha}_0^{ij}$ are given by

$$-\sum_{n}^{n_{\max}} L_{\mathrm{Fe}}^{\mathrm{Cr}}(\mathbf{q},\lambda)\,F_n(\mathbf{q})\,\delta\boldsymbol{\alpha}_n^{\mathrm{Fe\text{-}Cr}} = \delta B(\lambda) + \sum_{i,j>i} L_i^j(\mathbf{q},\lambda) \sum_{n}^{n_{\max}} F_n(\mathbf{q})\,\delta\boldsymbol{\alpha}_n^{ij}. \quad (2)$$

This over-estimated linear system is solved by restricting the pair index ij of the right member of Eq. (2) to Ni-Fe and Ni-Cr. We found that the matrices involved in Eq. (2), that link the vector $\delta\boldsymbol{\alpha}_0^{\mathrm{Ni\text{-}Fe}}$ and the vector $\delta\boldsymbol{\alpha}_0^{\mathrm{Ni\text{-}Cr}}$ to the dummy vector $\delta\boldsymbol{\alpha}_0^{\mathrm{Fe\text{-}Cr}}$ are diagonal dominant (a diagonal element corresponds to wavelengths of the same $\mathbf{q}$ vector). The vectors are thus almost colinear, and can be fairly accurately approximated by

$$\begin{aligned} \delta\boldsymbol{\alpha}_0^{\mathrm{Ni\text{-}Fe}} &\approx -0.025\,\delta\boldsymbol{\alpha}^{\mathrm{Fe\text{-}Cr}}, \\ \delta\boldsymbol{\alpha}_0^{\mathrm{Ni\text{-}Cr}} &\approx -0.15\,\delta\boldsymbol{\alpha}^{\mathrm{Fe\text{-}Cr}}. \end{aligned} \quad (3)$$

In summary, at this stage of the analysis, and dropping the variation symbol δ, the SRO parameters are given by

$$\begin{aligned} \boldsymbol{\alpha}_n^{\mathrm{Ni\text{-}Fe}} &\approx \boldsymbol{\alpha}_0{}^{\mathrm{Ni\text{-}Fe}} - 0.025\boldsymbol{\alpha}^{\mathrm{Fe\text{-}Cr}}, \\ \boldsymbol{\alpha}_n^{\mathrm{Ni\text{-}Cr}} &\approx \boldsymbol{\alpha}_0^{\mathrm{Ni\text{-}Cr}} - 0.15\boldsymbol{\alpha}^{\mathrm{Fe\text{-}Cr}}, \\ \boldsymbol{\alpha}_n^{\mathrm{Fe\text{-}Cr}}&. \end{aligned} \quad (4)$$

The next step of the data analysis will be to reduce the range of allowable values for the unknown parameters $\boldsymbol{\alpha}_n^{\mathrm{Fe\text{-}Cr}}$. This can be partially done, requiring physical solutions from cluster convex polyhedra algebra. For example, consider the probability of occurrence of a nth neighbor Cr-Cr pair, which in terms of the SRO parameters is given by

$$P_n^{\mathrm{Cr\text{-}Cr}} = c_{\mathrm{Cr}}^2 + c_{\mathrm{Cr}}c_{\mathrm{Ni}}\alpha_n^{\mathrm{Ni\text{-}Cr}} + c_{\mathrm{Cr}}c_{\mathrm{Fe}}\alpha_n^{\mathrm{Fe\text{-}Cr}} \geq 0.$$

In the case of the nearest-neighbor pair, if we substitute $\alpha^{\mathrm{Ni\text{-}Cr}}$ by $-0.141 - 0.15\alpha^{\mathrm{Fe\text{-}Cr}}$, it can be seen that any physical state corresponds to $\alpha^{\mathrm{Fe\text{-}Cr}} \geq 0.22$ and therefore $\alpha^{\mathrm{Ni\text{-}Cr}} \leq -0.174$, which is much lower than our initial guess. The extension of these considerations to larger cluster, namely, the tetrahedron octahedron (TO), give only lower or upper bounds on the $\alpha_n^{\mathrm{Fe\text{-}Cr}}$, so additional criteria are needed. These can come from consideration of the Ising model internal self-consistency.

The inverse CVM (ICVM) maps a set of short-range order $\boldsymbol{\alpha}$ onto a set of effective potentials $\mathbf{J}(\boldsymbol{\alpha})$, which is used as input in the CVM to deduce the thermodynamic properties of the system at other temperatures or other concentrations. For our problem, we add constraints to confine the available set of values for $\alpha^{\mathrm{Fe\text{-}Cr}}$, forcing the set of values for $\mathbf{J}(\boldsymbol{\alpha})$ to be compatible to the known results about the LRO and the decrease in the critical

temperature of Ni_3Fe upon Cr addition.

In a preceding paper,[15] we showed that both LRO and the change in critical temperature of dilute ternary alloys, are functions of a unique linear combination of the effective interactions $X_1 = (J_1^{Ni-Cr} - J_1^{Fe-Cr})/J_1^{Ni-Fe}$. This work was done using nn interactions (tetrahedron CVM), while the TO ICVM also involves next-nearest-neighbor (NNN) interactions. Adding the contribution of the second-nearest-neighbor interactions to our previous formalism can be done approximately by defining an effective nn pair that sums the effect of the nn and nnn pairs $J = J_1 + \lambda J_2$. In the binary $L1_2$ alloy, we substitute a ternary addition on each of the two sublattices of the $L1_2$ structure, with a probability proportional to the corresponding Boltzman factor, that is

$$P^{C/I} \propto e^{-\beta H_{C/I}}, \qquad P^{C/II} \propto e^{-\beta H_{C/II}}. \tag{5}$$

C/I stands for the substitution of the impurity C on sublattice I; $H_{C/I}$ is the resulting energy cost. The long-range order parameter for the impurity atoms, which measures the trend for atoms C to sit preferentially on one sublattice, is thus proportional to the difference $P^{C/I} - P^{C/II}$. Assuming that the degeneracy of the sublattice II is three, we find:

$$\eta_C \approx \frac{P^{C/I} - P^{C/II}}{P^{C/I} + 3P^{C/II}} \approx \frac{1 - e^{-\beta\Delta H}}{1 + 3e^{-\beta\Delta H}}. \tag{6}$$

In the above expression ΔH, which accounts for the energy difference between the two possible substitutions of the impurity C, can be estimated considering a perfectly ordered $L1_2$ structure, and we find $\lambda = -\frac{3}{2}$. Extending our conclusion in paper,[15] the measurement of η_{Cr} in a $(Ni_3Fe)_{0.964}Cr_{0.036}$ long-range ordered alloy,[16] and the lowering of T_c of Ni_3Fe when Cr is added,[12] show that the parameter

$$X = \frac{\left(J_1^{Ni-Cr} - \frac{3}{2}J_2^{Ni-Cr}\right) - \left(J_1^{Fe-Cr} - \frac{3}{2}J_2^{Fe-Cr}\right)}{\left(J_1^{Ni-Fe} - \frac{3}{2}J_2^{Ni-Fe}\right)}$$

is close to zero. Hence, in order to ensure the thermodynamic self-consistency with available LRO results, we constrained the parameter X to lie within the interval $[-0.5, 0.5]$, which is intermediate to the cases $X = \pm 1$, where the slope of the change in critical temperature upon ternary additions vanishes.

A plausible set of α's was finally obtained using the simplex algorithm to minimize the sum of the squares of the constraints. At each step of the algorithm, the ICVM is used to compute the J's from any set of α's. The results we have obtained in this way are summarized in Table II. As a by product of the minimization involving the ICVM, we have also computed the reduced susceptibility matrix that gives the order of magnitude of the variations of the effective interaction energies with respect to the variations of the α parameters. The coefficients of this matrix are also given in Table II. It can be seen that errors in the α^{Fe-Cr} parameters do not imply drastic errors in the effective energies.

VI. DISCUSSION

The variant of the ICVM, which we have described in the preceding section, simulates the first two SRO parameters associated to each pair. In this section, we would like to check the influence of the assumptions we made on the diffuse scattering itself. For that purpose, and also to study the behavior of the alloy with respect to temperature, it is convenient to use the canonical Monte Carlo (MO) method.

The MC runs were made on a $4\times16\times16\times16$ box (16 384 spins), applying periodic boundary conditions. The first 20 pair-correlation functions were computed over Markov chains about 3000 MC per spin, disregarding the first few hundred steps to allow for the thermalization of the system.

The results we obtained at the annealing sample temperature are listed in Table II, and as expected match the ICVM data. However, this result is not really significant in the sense that we already know that the CVM-TO and the MC method give almost identical results for temperatures a few percent above the transition temperature. More instructive is the comparison of the third

TABLE II. Effective pair energies, SRO parameters and their associated Jacobian matrix for a "plausible" solution.

	$(Ni\text{-}Fe)_1$	$(Ni\text{-}Cr)_1$	$(Fe\text{-}Cr)_1$	$(Ni\text{-}Fe)_2$	$(Ni\text{-}Cr)_2$	$(Fe\text{-}Cr)_2$
βJ_i	+0.382	+0.818	+0.231	−0.043	+0.088	−0.264
J_i meV	+23.7	+50.7	+14.3	−2.7	+5.5	−21.8
α_i^{CVM}	−0.152	−0.194	+0.360	+0.148	+0.035	+0.100
α_i^{MC}	−0.156	−0.196	+0.361	+0.163	+0.048	+0.096
$\frac{\partial\beta J_i}{\partial\alpha_1^{Ni-Fe}}$	−6.0	−4.1	−0.4	−1.2	−0.8	+0.1
$\frac{\partial\beta J_i}{\partial\alpha_1^{Ni-Cr}}$	−1.2	−15	−10	−0.3	−1.6	−0.3
$\frac{\partial\beta J_i}{\partial\alpha_1^{Fe-Cr}}$	−0.0	−3.4	−3.9	+0.0	−0.1	−0.1
$\frac{\partial\beta J_i}{\partial\alpha_2^{Ni-Fe}}$	−2.4	−1.7	+0.2	−1.6	−0.5	−0.5
$\frac{\partial\beta J_i}{\partial\alpha_2^{Ni-Cr}}$	−0.5	−3.2	−0.8	−0.1	−2.5	−1.5
$\frac{\partial\beta J_i}{\partial\alpha_2^{Fe-Cr}}$	−0.0	−0.2	−0.2	−0.0	−0.5	−1.1

and fourth SRO parameters, that can be made from the MC data and Eq. (4) as follows:

$$\alpha_{MC}^{Ni-Fe} = \alpha_0^{Ni-Fe} - 0.025\alpha_{MC}^{Fe-Cr},$$

$$\alpha_{MC}^{Ni-Cr} = \alpha_0^{Ni-Cr} - 0.15\alpha_{MC}^{Fe-Cr}.$$

We have found that within the limit of the accuracy given in Table I, the above relations are fairly well approximated. The same argument, applied to more distant neighbors become less significant but shows that the trend is fulfilled. A typical snapshot of the equilibrium configurations sampled at this temperature is given in Fig. 7. As it can be seen, the SRO looks homogeneous through the box, whereas the sequence of SRO parameters would have inclined us to view the SRO state as a phase separation into small $L1_2$ and DO_{22} domains. This shows that the realm of ternary alloys cannot be simply analyzed in term of the binary components. In fact, the effective pair energies given in Table II do not reflect the symmetry of a ternary alloy around the stoichiometry $(\frac{1}{3}, \frac{1}{3}, \frac{1}{3})$. These are only linear combinations of the pair-correlation functions conjugated energies. For example, setting one of these J to zero does not imply that the corresponding α will vanish. The behavior of the first four order SRO parameters with respect to temperature are shown in Fig. 8. The sharp variations of these parameters in the neighborhood of the reduced temperature $\frac{T}{T_{exp}} = 0.72$, correspond to the crossing of a transition line. This dimensionless parameter corresponds to the temperature 248 °C, which is lower than the value extrapolated from the data of Marwik, Piller and Cranshow.[13] This minor disagreement could be a result of the simplification involving the second-neighbor interactions in the ICVM analysis.

In Fig. 9, we display a snapshot of the configurations sampled at the low temperature of $\frac{T}{T_{exp}} = 0.5$. This configuration maps the ground state of the alloy, and clearly exhibits two ordered phases. This corresponds to the phase separation of the $L1_2(Ni_3Fe)$ and $DO_{22}(Ni_3Cr)$ phases. This intuitive result, considering the sequence of binary SRO parameters, means that there are no other competing ground states around the chosen composition.

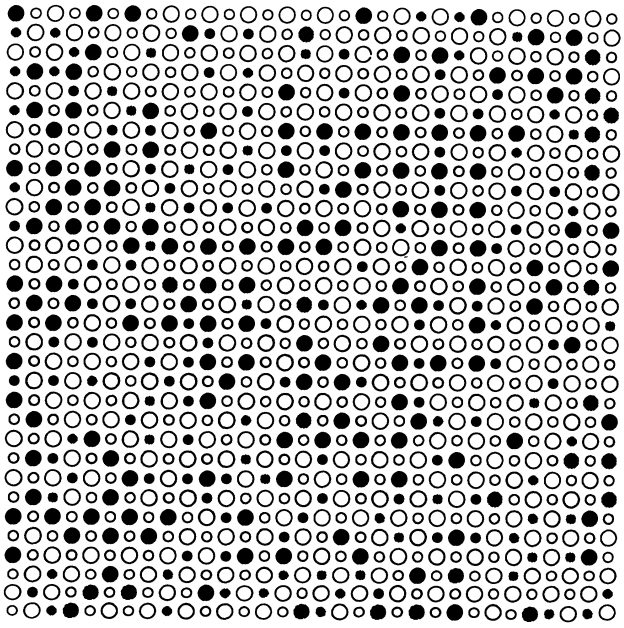

FIG. 7. Snapshot of a typical configuration, which contributes to the thermal equilibrium SRO state at the experimental temperature. As can be seen, and as checked over many such configurations, there are no domains which correspond to a microstructure of the alloy.

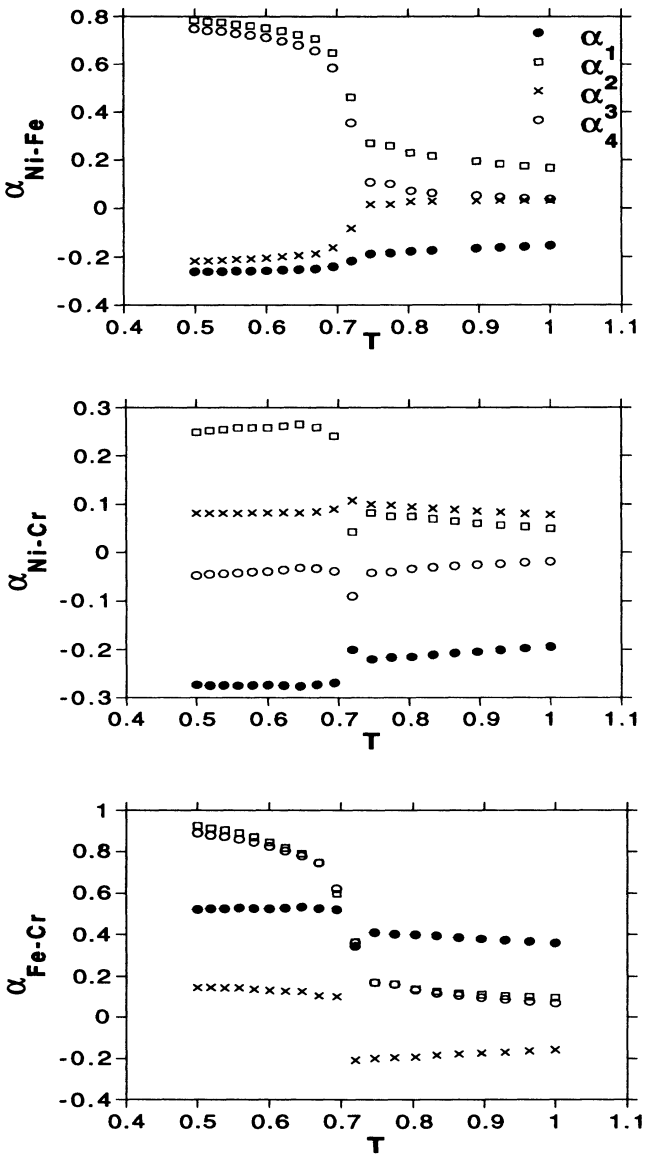

FIG. 8. Variations of the α parameters with the dimensionless temperature. The experimental temperature corresponds to $T = 1$. The sharp variations of the α's at $T \approx 0.72$ signals the occurrence of a transition. The data close to the transition temperature should be considered with care as the specific-heat curve (not reproduced here) indicates that long-life metastable states may have been trapped.

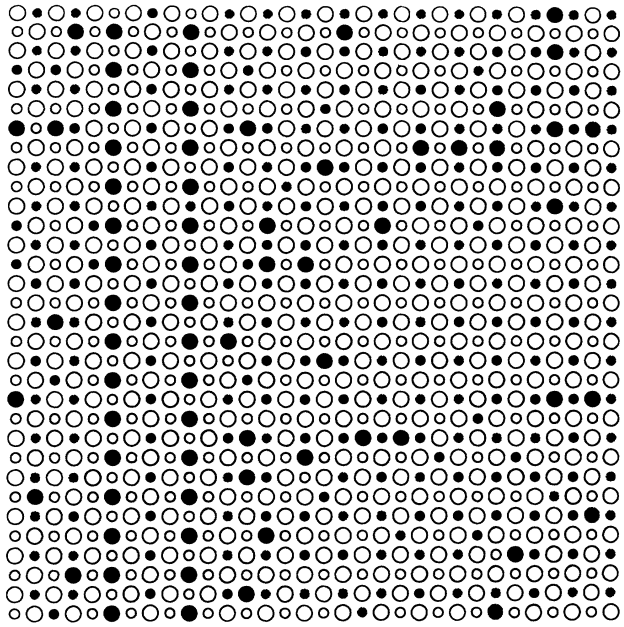

FIG. 9. Snapshot of a low-temperature configuration $T = 0.5$. At this temperature, the picture reveals a phase separation between the $L1_2$ (Ni_3Fe) and the DO_{22} (Ni_3Cr) structures. At lower temperatures, it is expected that the remaining randomly distributed chromium atoms will gather in a thicker IPB to accommodate the off-stoichiometry, while lowering the excess free energy.

The overall mapping of the diffuse scattering intensity at temperatures above the transition temperature displays the decomposition of the concentration waves. In Fig. 10, we have mapped the behavior of the diffuse scattering intensity for Ni-Cr and Fe-Cr pairs on crossing the disorder-order transition temperature. The diffuse intensity from the Ni-Fe pairs is not shown: it simply concentrates into sharp [100] maxima.

The diffuse scattering from the Ni-Cr pairs is sensitive to the $[1\frac{1}{2}0]$ concentration wave, the spots being elongated along [100] direction. As the temperature is lowered, the maximum becomes narrower and even splits into two spots at the transition temperature, and then at a lower temperature the [100] wave appears.

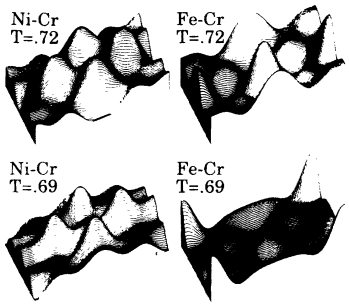

FIG. 10. Diffuse scattering intensity maps for the two partial Ni-Cr and Fe-Cr, above and below the transition temperature. The Ni-Cr pair intensity evolves as the DO_{22} structure and the emergence of the $\langle 100 \rangle$ wave in addition to the $\langle 1\frac{1}{2}0 \rangle$ wave is clearly seen. The Fe-Cr pair intensity gathers into the Bragg peaks at low temperature. It should be noticed that the maxima and the minima between the Ni-Cr and the Fe-Cr intensities are in an almost one to one correspondence to ensure the positive definition of the total intensity.

The diffuse scattering from the Fe-Cr is gathered into Bragg peaks, and shows splitting around the [100] wave maxima. As the temperature is lowered, the splitting stretches and finally disappears at temperatures close to the transition temperature.

Below the transition temperature, all the intensity gathers into the Bragg peaks.

For all temperatures the total intensity is dominated by the Ni-Fe pair partial intensity, and the $[1\frac{1}{2}0]$ maxima are not present. This is due to mutual cancellation of the intensity extrema between Ni-Cr and Fe-Cr pairs. In a ternary alloy, only the total diffuse scattering intensity has to be positive definite. In a finer analysis of the diffuse intensity map we found that to maxima of the intensity relative to Ni-Cr pairs correspond negative minima of the intensity of Fe-Cr, while simultaneously Ni-Fe plays a symmetric role with Fe-Cr pairs. The splitting of the maxima of the two partial Ni-Cr and Fe-Cr might result from different rates to reach thermal equilibrium between the $L1_2$ and DO_{22} phases.

VII. CONCLUSION

In this paper, we have described an original method of analyzing the diffuse scattering for dilute ternary alloys, where conventional experimental analysis techniques fail. The method uses the self-consistence of the Ising model, and assumes the transferability of the effective energies to different temperatures, at least for nonmagnetic systems. The method includes the experimental knowledge about LRO to determine a plausible set of SRO parameters. As a by-product the method gives the effective pair potentials, which we have been able to use in the Monte Carlo simulations. We have shown that, in contrast to the intuitive picture from the sequence of SRO parameters, the experimental diffuse scattering corresponds to a homogeneous distribution of the species in the solid solution, without specific microstructure.

The behavior of the alloy as a function of temperature has also been studied. The ground state of the alloy corresponds to the order-order phase separation of the binary Ni_3Fe $L1_2$ structure, and of the binary Ni_3Cr DO_{22} structure. The diffuse scattering intensity maps have revealed some specific features of ternary alloys, such as negative contributions of some partial to the total intensity.

The analysis of ternary solid solution will always remain a difficult problem because except in a few cases some necessary information will always be missing. However, this paper shows that theoretical tools can be designed to get rid of the problems associated with this lack of information.

ACKNOWLEDGMENTS

The authors are pleased to acknowledge the C.P.R "Stabilité Structurale des Superalliages Monocristallins" for financial support.

APPENDIX A: CALCULATION OF THE TDS CONTRIBUTION

In this appendix, we describe in some details a new method to analyze the contribution of the thermal diffuse scattering (TDS) to the diffuse intensity. The method is based upon the diagonalization of the dynamical matrix and takes the alloy elastic constants into account. This analysis is expected to improve upon the "classical" treatment of the TDS correction for experiments done at temperatures lower than the alloy Debye temperature. Before discussing this method, let us briefly review the basic definitions and the main steps in analyzing the diffuse intensity.

According to Warren,[29] the scattered intensity for a homogeneous solid solution can be written [in electronic units (eu)]

$$I_{\mathrm{eu}} = \sum_{A,B,n} f_A^* f_B \left(C_A C_B + X_n^{AB}\right) \times e^{i\mathbf{q}\mathbf{R}_n} e^{-\langle[\mathbf{q}\left(\mathbf{U}_n^B - \mathbf{U}_0^A\right)^2]\rangle/2}, \quad \text{(A1)}$$

where f_A is the scattering factor for atom A, C_A is the concentration of atoms A, X_n^{AB} is the pair correlation function for the nth neighbor pair AB, A sitting at an arbitrary origin, $\mathbf{q}$ is the scattering vector, and $\mathbf{U}_n^A$ is the instantaneous position vector measured from the lattice position $\mathbf{R}_n$. The argument of the second exponential factor in (A1), which should be time averaged ($\langle\,\rangle$), can be written as:

$$-\frac{\langle[\mathbf{q}\left(\mathbf{U}_n^B - \mathbf{U}_0^A\right)^2]\rangle}{2} = -\frac{\langle\left(\mathbf{q}\mathbf{U}_0^A\right)^2\rangle}{2} - \frac{\langle\left(\mathbf{q}\mathbf{U}_n^B\right)^2\rangle}{2} + \langle\left(\mathbf{q}\mathbf{U}_0^A\right)\left(\mathbf{q}\mathbf{U}_n^B\right)\rangle. \quad \text{(A2)}$$

Using Eq. (A2), the first-order Taylor expansion of the total intensity with respect to $\langle\left(\mathbf{q}\mathbf{U}_0^A\right)\left(\mathbf{q}\mathbf{U}_n^B\right)\rangle$ is given by

$$I_{\mathrm{eu}} = \sum_{A,B,n} \tilde{f}_A^* \tilde{f}_B \left(C_A C_B + X_n^{AB}\right) \times e^{i\mathbf{q}\mathbf{R}_n}\left(1 + \langle\left(\mathbf{q}\mathbf{U}_0^A\right)\left(\mathbf{q}\mathbf{U}_n^B\right)\rangle\right), \quad \text{(A3)}$$

$\tilde{f}_A = f_A e^{-\frac{\langle\left(\mathbf{q}\mathbf{U}^A\right)^2\rangle}{2}}$ being the scattering factor of atom A, corrected for the Debye-Waller factor.

Finally, having expanded the sum argument in (A3), we can make explicit the contributions of the Bragg intensity (I_B), of the short-range order intensity (I_{SRO}) and the TDS intensity of the completely disordered alloy for the one-phonon approximation. The diffuse intensity can therefore be written

$$I = I_B + I_{\mathrm{SRO}} + I_{\mathrm{TDS}_1}, \quad \text{(A4)}$$

$$I_B = \mid \sum_A C_A \tilde{f}_A \mid^2 \delta\left(\mathbf{q} - \mathbf{K}\right),$$

$$I_{\mathrm{SRO}} = \sum_{A<B} C_A C_B \mid \tilde{f}_A - \tilde{f}_B \mid^2 \sum_n \alpha_n^{AB} e^{(i\mathbf{q}\mathbf{R}_n)},$$

$$I_{\mathrm{TDS}_1} = \sum_{A,B} C_A C_B \tilde{f}_A^* \tilde{f}_B \sum_n e^{(i\mathbf{q}\mathbf{R}_n)} \langle\left(\mathbf{q}\mathbf{U}_n^B\right)\left(\mathbf{q}\mathbf{U}_0^A\right)\rangle.$$

The above equation for the total diffuse intensity should normally involve a fourth term I_{TDS_2} which accounts for the correction to I_{TDS_1} due to the short-range order. As a first approximation, we may neglect this term as its contribution is scaled by a Laue factor, while I_{TDS_1} is scaled by a structure factor term.

At this level of approximation, the vector $\mathbf{U}_n^A$, which describes the atomic motion of the atom A around its equilibrium lattice position $\mathbf{R}_n$, is given by[30]

$$\mathbf{U}_n^A = \sum_{i\mathbf{g}} \sqrt{\frac{2E_{i\mathbf{g}}}{N m_A \omega_{i\mathbf{g}}^2}} \mathbf{e}_{i\mathbf{g}} \cos\left(\mathbf{g}\mathbf{R}_n - \omega_{i\mathbf{g}} t + \Phi_{i\mathbf{g}}\right). \quad \text{(A5)}$$

In equation (A5), $E_{i\mathbf{g}}, \omega_{i\mathbf{g}}, \Phi_{i\mathbf{g}}$ and $e_{i\mathbf{g}}$ are, respectively, the mean energy, the frequency of oscillation, the random phase and the polarization vector associated with the wave mode $i\mathbf{g}$, where $i = 1, 2, 3$ and $\mathbf{g}$ belongs to the first Brillouin zone.

In the case of a lattice with cubic symmetry, if we assume spring forces between the nearest neighbor, we may assign to each mode $\mathbf{g} \equiv (g_1, g_2, g_3)$ a dynamic matrix D whose elements are defined in terms of the elastic constant C_{11}, C_{12}, C_{44} and of the lattice parameter a by the following equations:

$$D_{ii}(\mathbf{g}) = aC_{11}\{2 - \cos\left(\pi g_i\right)\left[\cos\left(\pi g_j\right) + \cos\left(\pi g_k\right)\right]\} + a\left(2C_{44} - C_{11}\right)\left[1 - \cos\left(\pi g_j\right)\cos\left(\pi g_k\right)\right],$$

$$D_{ij}(\mathbf{g}) = a\left(C_{12} + C_{44}\right)\sin\left(\pi g_i\right)\sin\left(\pi g_j\right). \quad \text{(A6)}$$

The dynamical matrix D is then diagonalized and $\omega_{i\mathbf{g}}^2$ and $\mathbf{e}_{i\mathbf{g}}$ are the corresponding eigenvalues and eigenvectors. The time-averaged factor in Eq. (A4) can then be evaluated as

$$\langle\left(\mathbf{q}\mathbf{U}_n^B\right)\left(\mathbf{q}\mathbf{U}_0^A\right)\rangle = \frac{m}{N\sqrt{m_B m_A}} \times \sum_{i\mathbf{g}} \frac{E_{i\mathbf{g}}}{m\omega_{i\mathbf{g}}^2}\left(\mathbf{q}\mathbf{e}_{i\mathbf{g}}\right)^2 \cos\left(\mathbf{g}\mathbf{R}_n\right), \quad \text{(A7)}$$

$$m = \sum_A C_A m_A.$$

In the above expression, the sum is only once over the index i and $\mathbf{g}$ as the time average of the cross products of cosine factors associated to different wave modes cancel owing to the randomness of the phase factors. Substituting Eq. (A7) in Eq. (A4), and using the symmetry property of the dynamic matrix with respect to the inversion of the $\mathbf{g}$ vectors, we find that the TDS intensity factor can be written

$$I_{\mathrm{TDS}_1}(\mathbf{q}) = \sum_{A,B} \tilde{f}_A^{\star} \tilde{f}_B C_A C_B \frac{m}{\sqrt{m_A m_B}} \sum_{\mathbf{ig}} \frac{E_{\mathbf{ig}}}{m\omega_{\mathbf{ig}}^2} (\mathbf{q}\mathbf{e}_{\mathbf{ig}})^2 \left(\frac{1}{N} \sum_n e^{(\mathbf{q}\mathbf{R}_n)} \cos(\mathbf{g}\mathbf{R}_n) \right) \tag{A8}$$

$$= \left| \sum_A \frac{\sqrt{m} C_A \tilde{f}_A}{\sqrt{m_A}} \right|^2 \sum_{\mathbf{ig}} \frac{E_{\mathbf{ig}}}{m\omega_{\mathbf{ig}}^2} (\mathbf{q}\mathbf{e}_{\mathbf{ig}})^2 .$$

This final expression for I_{TDS_1} shows the following.

(1) The first-order thermal diffuse scattering is not exactly proportional to the square of the atomic scattering factor, and that the atomic scattering factor has to be weighted by the square root of the inverse of the relative atomic mass, i.e., $\sqrt{\frac{m}{m_A}}$.

(2) The first-order thermal diffuse scattering increases quadratically with respect to the scattering vector $\mathbf{q}$. The average energy of the wave mode $i\mathbf{g}$ given from the Bose-Einstein statistic is $E_{i\mathbf{g}} = \hbar\omega_{i\mathbf{g}}[\frac{1}{2} + 1/(e^{\hbar\omega_{i\mathbf{g}}/kT} - 1)]$. In the classical approximation,[24] we substitute kT for $E_{i\mathbf{g}}$, which require that the condition $kT \ll \hbar\omega_{i\mathbf{g}}$ is met. This approximation is justified for the $\mathbf{g}$ associated to the acoustic modes near the origin of the first Brillouin zone if the measurements are made at high temperatures. However, the relevant diffuse scattering lies between the Bragg peaks, and for a vector $\mathbf{g}$ close to the limit of the first Brillouin zone, $\hbar\omega_{i\mathbf{g}}$ is of the order of magnitude of the Debye temperature $k\Theta_D$. In our case, where $\Theta_D = 450$ K and $T = 100$ K, we found the quantum correction factor $\frac{E_{i\mathbf{g}}}{kT}$ may be as large as 2.3, making the classical approximation invalid.

A correction factor to the proportionality between I_{TDS_1} and kT have been proposed by Borie,[31] which require measurements to be made at two different temperatures but which is still based upon the assumption $\frac{\hbar\omega_{i\mathbf{g}}}{kT} \ll 1$.

The method we have described gets rid of these difficulties and satisfactorily takes into account the dispersion relationship for highly symmetrical directions. This new correction scheme only requires for a little additional computational effort, namely, the diagonalization of the dynamic matrix.

[1] V. Gerold and J. Kern, Acta. Metall. **35**, 393 (1987).
[2] D. Gratias and P. Cenedese, J. Phys. (Paris) Colloq. **45**, C9-149 (1985); see also P. Cenedese, A. Marty, and Y. Calvayrac, J. Phys. (Paris) **50**, 2193 (1989).
[3] P. Cenedese, F. Bley, and S. Lefebvre, Acta Crystallogr. A **35**, 228 (1984).
[4] S. Hashimoto, H. Iwasaki, K. Ohshima, J. Harada, M. Sakata, and H. Terauchi, J. Phys. Soc. Jpn. **54**, 3796 (1985).
[5] I. Mirebeau, M. Hennion, and G. Parette, Phys. Rev. Lett. **53**, 687 (1984).
[6] L. Reinhard, J. L. Robertson, S. C. Moss, G. E. Ice, P. Zschack, and C. J. Sparks, Phys. Rev. B **45**, 2662 (1992).
[7] B. Schönfeld, L. Reinhard, G. Kostorz, and W. Bührer, Phys. Status Solidi B **148**, 457 (1988).
[8] W. Schweika and H. G. Haubold, Phys. Rev. B **37**, 9240 (1988).
[9] M. Sarfati, Thèse de l'Université Paris-Sud, Orsay, 1991.
[10] S. Lefebvre, F. Bley, M. Fayard, and M. Roth, Acta. Metall. **29**, 749 (1981).
[11] G. E. Ice, C. J. Sparks, A. Habenschuss, and L. B. Shaffer, Phys. Rev. Lett. **68**, 863 (1992).
[12] H. Ferjani, F. Bley, and Y. Calvayrac, J. Phys. (Paris) Colloq. **38**, C7-55 (1977).
[13] A. D. Marwick, R. C. Piller, and T. E. Cranshow, J. Phys. F **17**, 37 (1987).
[14] V. I. Gomankov and N. I. Nogin, Phys. Met. Metall. **52**, 192 (1981).
[15] A. Marty, Y. Calvayrac, F. Guillet, and P. Cenedese, Phys. Rev. B **44**, 11 640 (1991).
[16] A. Marty, M. Bessière, F. Bley, Y. Calvayrac, and S. Lefebvre, Acta. Metall. **38**, 345 (1990).
[17] M. Bessière, G. Bessenay, J. Frouin, M. Jouvin, and S. Lefebvre, Nucl. Instrum. Methods Phys. Res. A **261**, 591 (1987).
[18] E. Elkaïm, S. Lefebvre, R. Kahn, J. F. Bérar, M. Lemonnier, and M. Bessière, Rev. Sci. Instrum. **63** (1), 988 (1992).
[19] F. Chassagne, M. Bessière, Y. Calvayrac, P. Cenedese, and S. Lefebvre, Acta. Metall. **37**, 2329 (1989).
[20] P. A. Doyle and P. S. Turner, Acta Crystallogr. A **24**, 390 (1968).
[21] S. Sasaki, KEK Report No. 83-22, 1984 (unpublished).
[22] D. T. Cromer and J. B. Mann, J. Chem. Phys. **47**, 1892 (1967).
[23] D. T. Cromer, J. Chem. Phys. **50**, 4857 (1969).
[24] C. B. Walker and D. R. Chipman, Acta Crystallogr. A **24**, 447 (1970).
[25] P. Turchi, Y. Calvayrac, and F. Plique, Phys. Status Solidi A **5**, 229 (1978).
[26] P. C. Clapp and S. C. Moss, Phys. Rev. **142**, 418 (1966).
[27] J. M. Sanchez, Physica A **111**, 200 (1982).
[28] F. Guillet, Thèse de l'Université ParisVI, Paris, 1993.
[29] B. E. Warren, in *X-Ray Diffraction* (Addison-Wesley, Reading, 1969).
[30] B. T. M. Willis and A. W. Pryor, in *Thermal Vibration in Crystallography* (Cambridge University Press, Cambridge, England, 1975).
[31] B. Borie, Acta Crystallogr. **17**, 212 (1964).

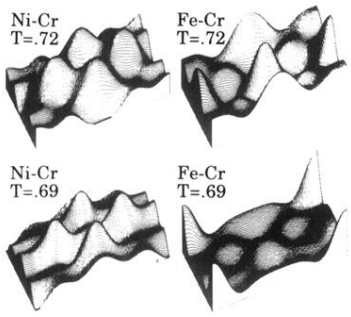

FIG. 10. Diffuse scattering intensity maps for the two partial Ni-Cr and Fe-Cr, above and below the transition temperature. The Ni-Cr pair intensity evolves as the DO_{22} structure and the emergence of the $\langle 100 \rangle$ wave in addition to the $\langle 1\frac{1}{2}0 \rangle$ wave is clearly seen. The Fe-Cr pair intensity gathers into the Bragg peaks at low temperature. It should be noticed that the maxima and the minima between the Ni-Cr and the Fe-Cr intensities are in an almost one to one correspondence to ensure the positive definition of the total intensity.